A Modernized ANSYS-Based Finite Element Model for the Thermal-Electrical Design of Aluminum Reduction Cells

Daniel Richard[1], André Felipe Schneider[2], Marc Dupuis[3], Stephan Broek[4]
1. Associate – Center of Excellence for Aluminum, Hatch Ltd., Saguenay, Canada
2. Numerical Analysis Specialist – Center of Excellence for Aluminum, Hatch Ltd., Montréal, Canada
3. Consultant, GeniSIM, Inc., Saguenay, Canada
4. Director – Center of Excellence for Aluminum, Hatch Ltd., Mississauga, Canada

Corresponding author: daniel.richard@hatch.com

Abstract

Heat balance and magnetohydrodynamics are critical to the design of an aluminum reduction cell since they largely determine its operational window. An inadequate lining design generally leads to degraded cell performance and premature failures. The first task in lining design is to determine the position of the frozen ledge and the cell superheat for a range of operational parameters.

Although several different modeling approaches and computational domains have been proposed to solve the Stefan problem, a widely accepted methodology, first proposed by Dupuis [1], is based on the iterative repositioning of the ledge front in a thermoelectrical (TE) Finite Element (FE) model. The algorithm involves successive displacements of the solidification front nodes based on the calculated temperature field until the entire ledge-to-liquids interface reaches the bath solidification temperature. The superheat is adjusted to minimize the difference between the cell internal heat and the integrated heat losses over the control volume. Originally, this approach was limited to two layers of first order elements across the ledge thickness moving horizontally and did not include the liquids.

This paper presents a generalization and a modernization of the original methodology, enabling the prediction of the ledge profile using an arbitrary number of first or second order elements through the ledge thickness while including the metal pad and the bath. The proposed modeling framework has been implemented in ANSYS using the APDL scripting language and designed to minimize the computational cost of moving the ledge. The generic core macros also efficiently handle the ledge front displacement in any orientation. Current technology ANSYS elements are used, such that high-performance computing solvers can be leveraged.

The robustness of our approach is illustrated using a fictitious 300 kA demonstration technology and compared with the standard approach.

Keywords: Aluminum reduction cells, heat balance, moving ledge profile, Finite Element analysis.

1 Introduction

Hatch has long been involved in the assessment of aluminium reduction technologies for greenfield and brownfield smelter projects and has recently been mandated to evaluate designs for a brownfield retrofit project, and specifically to perform heat balance calculations. Numerical modeling is the best tool to study the thermal-electrical behavior of the lining, and the basic methodology is mature and widely accepted.

Dupuis first developed a FORTRAN routine to reposition the ledge profile of a cathode slice and then solve the new geometry with a finite element analysis in the commercial software ANSYS. The approach was then implemented in the ANSYS interpreted scripting language APDL [1]. The model domain was progressively enlarged to include a full quarter cell [2] but did not include the liquids. The electrical boundary conditions were applied to the immerged surface of the anodes and to the surface of the cathode blocks as an electrical equipotential.

Dupuis introduced a full cell slice (*i.e.* including the anode and the cathode) with combined convergence of cell superheat and the ledge profile in [3]. The liquid zone for the full quarter was introduced in [4] to obtain a representative current distribution in the metal pad.

Essentially, the same modeling approach was used by Dupuis to move the ledge from the mid-1980's up to his most recent work in 2019 [5]. In that period, the ANSYS software platform has evolved and some of the functionalities used by Dupuis are now deprecated and not compatible with the most recent versions.

Also, the authors agree that some of the drawbacks of the original Dupuis approach are the following:

- The construction of the geometry is from the bottom-up and requires experience with ANSYS APDL;
- The discretization of the domain is limited to linear elements;
- The ledge thickness is limited to 2 elements;
- The ledge mesh is attached to the cathode surface, which is limiting for the construction of the corner geometry, and limits the position of the ledge toe as it depends on the cathode block assembly topology;
- The processing time for moving ledge and apply updated boundary conditions is substantial;
- The models are based on legacy ANSYS elements:
  - The application of thermal loads directly on the elements is no longer supported;
  - These elements do not support present-day Distributed Memory Parallel (DMP) processing, which substantially increases computational performance of large models.

For all these reasons, the original approach was modernized and implemented in ANSYS 2020 R1.

2 Modernized Approach Workflow

The new workflow is summarized in Figure 1.

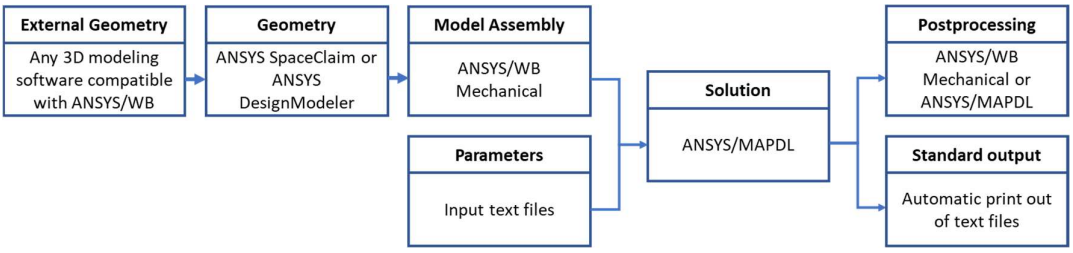

Figure 1. Modernized approach workflow.

2.1 External Geometry

Solid geometry can be developed in any package compatible with the ANSYS geometry engines and imported for further processing, for example using CATIA, Parasolid, STL, and STEP files.

2.2 Geometry Editing

The geometry that is tied to the model assembly is built with either ANSYS/SpaceClaim or ANSYS/Design Modeler. Within the context of the present work, the Authors used SpaceClaim to preprocess the geometry. External components can be imported and modified, and additional entities (e.g. the ledge) can be added directly in this module. Bodies are regrouped into parts that share a mesh, while the interaction between different parts is handled by contact-target element pairs when building the finite element model itself.

2.3 Finite Element Model Assembly

The geometry is linked into ANSYS Workbench/Mechanical, where the finite element (FE) mesh is built, contact is established between parts that do not share a mesh, and named components are defined.

The ANSYS/WB Mechanical environment is shown in Figure 2. The colors represent the different parts in the model that will share a mesh. Contact and target elements are used to transfer heat and electricity across non-matching meshes from the different parts, which facilitate the discretization of the domain.

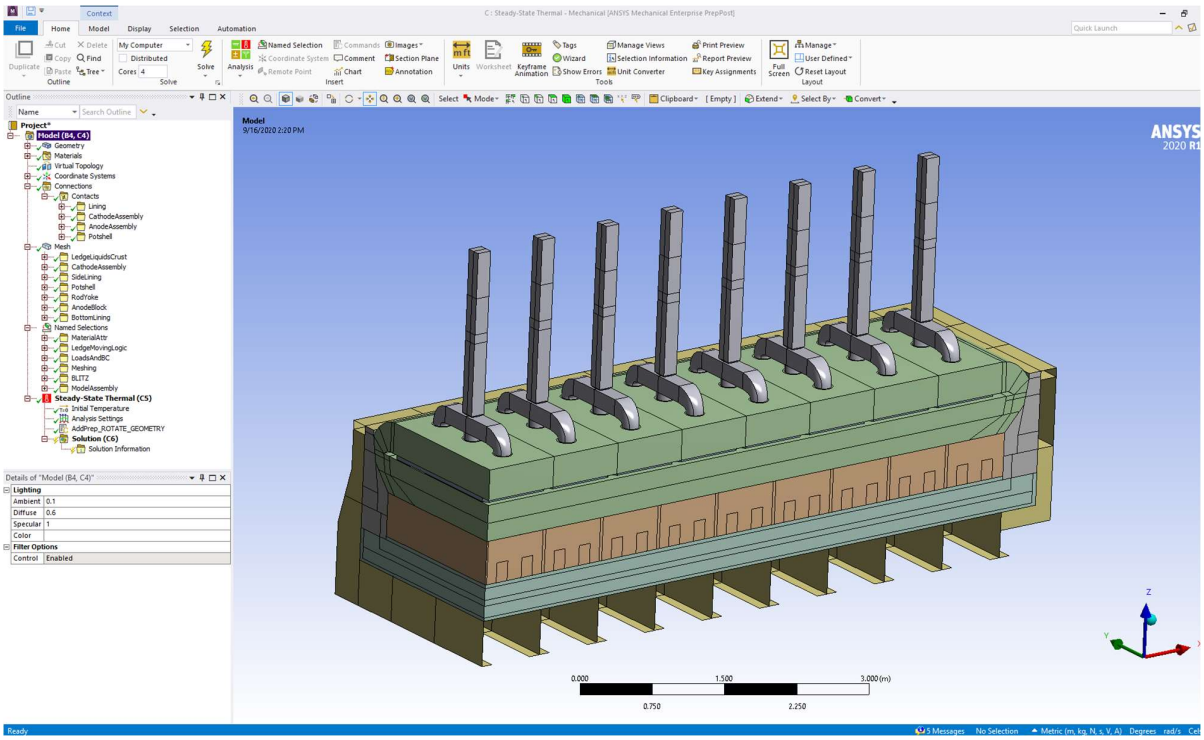

Figure 2. ANSYS Workbench/Mechanical environment with quarter cell model.

Named selections (or, simply, components) are used in APDL routines to:

- Assign materials properties;
- Assign element types and physics (e.g. thermal shell, thermal-electrical solid, etc.);
- Define contact and target surfaces;

- Apply boundary conditions, like surface convection or prescribed voltages;
- Define the entities required for the ledge repositioning logic;
- Define the heat balance control volume;
- Define the reference location for reporting the anodic and cathodic voltage drops;
- Define the boundaries of the cell control volume at the anodic and cathodic panels;
- Define the bodies included in the finite element solution but that are outside of the cell control volume;
- Define the surfaces for the detailed heat losses output;
- Define model assemblies for different types of solution (e.g. half anode, quarter anode panel, cathode slice, full cell slice, quarter cathode panel and full cell quarter).

Examples of named selections can be found in Figure 3. A typical FE mesh is shown in Figure 4, with coloring corresponding the element types.

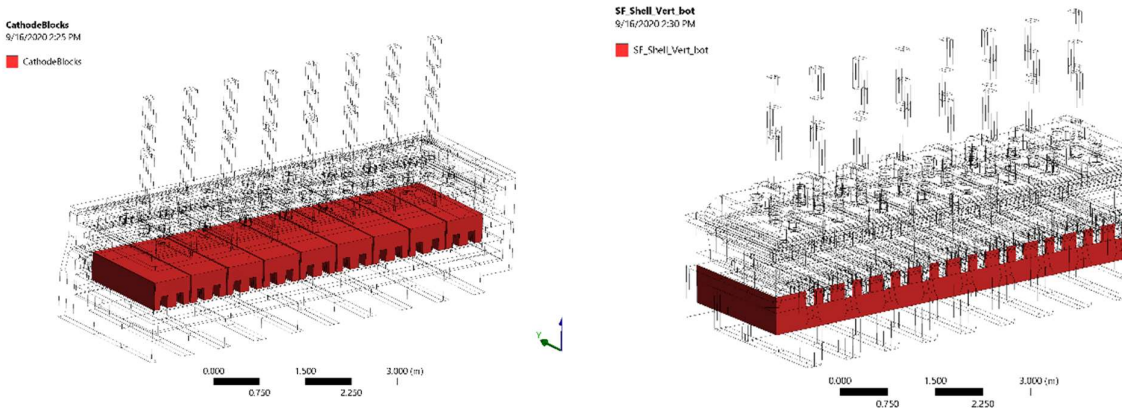

a) Material properties attribution: component identifying the cathode blocks.

b) Surface heat transfer load application: named selection identifying the lower part of the pot shell for convection and radiation.

Figure 3. Example of named selections (or components).

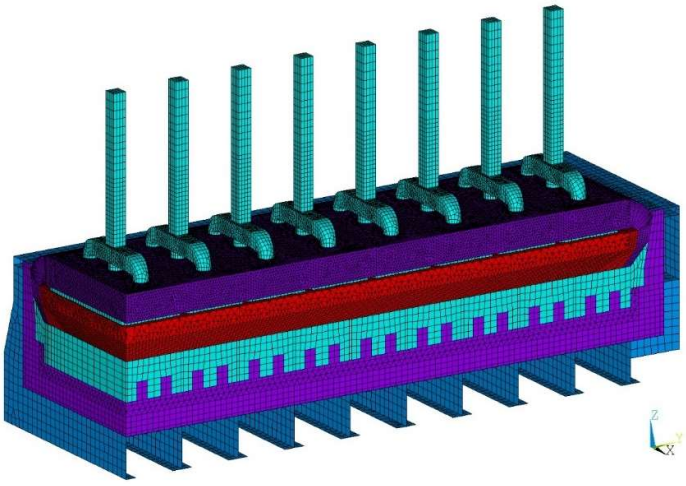

Figure 4. Full Quarter Initial Finite Element Linear Mesh.

2.4 Parameters

Once the mesh is built and all the components are defined, the user needs to update the input text files required for the solution. Model parameters defined in text files will be read by ANSYS/APDL routines. For example, the User Inputs are organized into four (4) main files:

- **General parameters**. This includes for example the cell amperage, the bath chemistry, the ambient temperature, the model domain and the type of solution.
- **Materials and physics.** This is where the material properties are assigned to named components, and a physics is selected.
- **Boundary conditions.** This is where convection and radiation heat transfer surface loads are defined by the user and assigned to named components.
- **Heat losses output definition.** This file is used to list the named components that will be used for the detailed heat losses standardized output.

2.5 Solution

Generic APDL macros are used to process the ANSYS Workbench database and the four (4) input text files. This can be done either interactively within the ANSYS/WB Mechanical module, or separately as a batch solution running in the background. Note that the user does not need to touch any of the generic macros to run the model.

The following steps occur during this phase:

- Read the ANSYS Workbench database;
- Read the general parameters;
- Reselect the appropriate model domain;
- Create and read the materials properties;
- Assign the material properties and the element types;
- Create the required contact and target element pairs;
- Create the auxiliary data structures for the ledge repositioning logic;
- Create the heat transfer coefficients;
- Apply the heat transfer loads and the electrical boundary conditions;
- Read the surfaces for the heat losses detailed output;
- Define the extrapolation factors required for the complete cell output heat losses corresponding to the model domain;
- Apply the settings for the nonlinear thermal-electrical solution;
- Solve the problem, either:
  - Static solution for half anode and anode panel models (i.e. thermal-electrical problem solved only once);
  - Ledge convergence only for cathode slice and quarter cathode models at fixed superheat;
  - Simultaneous superheat and ledge convergence for full cell slice and full cell quarter models.

2.6 Postprocessing

Postprocessing can either be programmed in APDL macros or done interactively in ANSYS. A typical temperature distribution is shown in Figure 5.

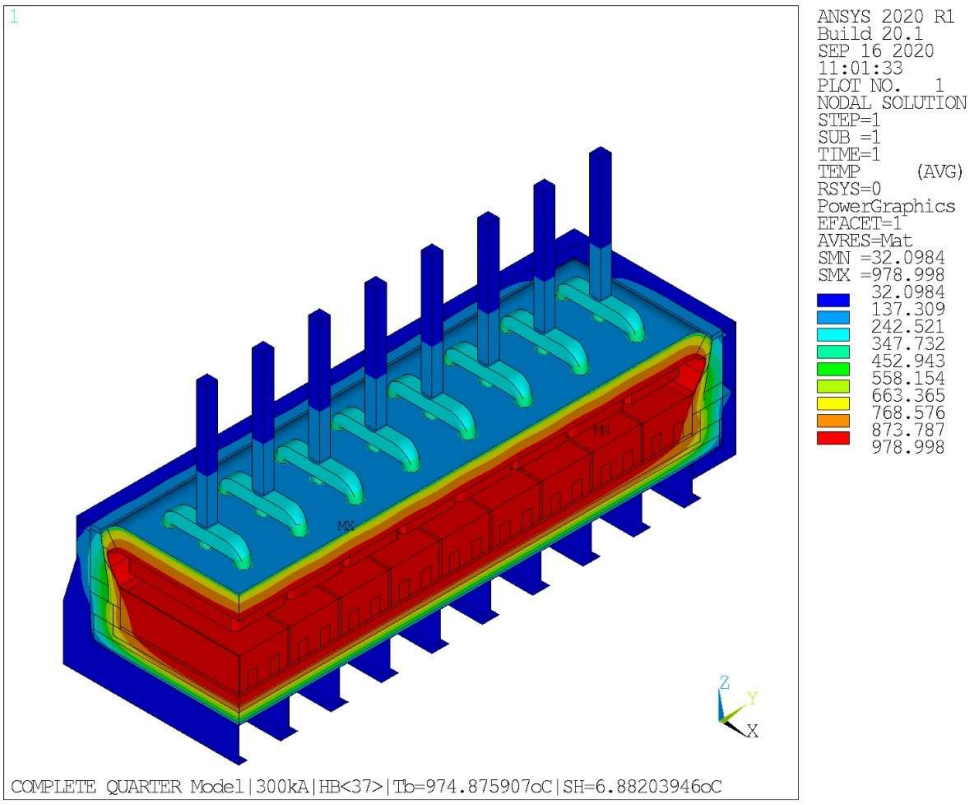

Figure 5. Full quarter cell temperature distribution in °C at converged ledge and superheat.

2.7 Standard Output

Once the global problem is converged, a standard output text file is created that summarizes the results and details the heat losses on the previously defined surfaces. An example is shown in Figure 6 for a quarter cathode model (*i.e.* no anode panel) ledge convergence solution using a quadratic FE mesh. Note that the detailed heat losses are reported for the model domain, so the user must multiply the heat flow by the appropriate scaling factor for the cell (in this case, by 4 since this is a quarter model).

```
============================================================
       CATHODE QUARTER Model
       Solution type  Ledge convergence only
============================================================

OPERATING CONDITIONS
------------------------------------------------------------
  Cell Current                [kA]    300.00
  Operating Temperature       [oC]    975.00
  Liquidus                    [oC]    968.00
  Superheat                   [oC]      7.00
  Ambient temperature         [oC]     20.00
============================================================

HEAT IN
------------------------------------------------------------
  Bath to ledge               [kW]     83.29
  Metal to ledge              [kW]    173.78
  Metal to lining             [kW]     53.87
  Joule Heat in Cathode       [kW]     91.92
```

```
  Total Heat into Cathode     [kW]    402.87
  Cathode Voltage Drop        [mV]    295.09
============================================================

GLOBAL HEAT LOST
------------------------------------------------------------
  Cathodic Panel              [kW]    402.826818
------------------------------------------------------------

DETAILED HEAT LOST OVER MODEL DOMAIN
------------------------------------------------------------
    [W]         [W/m2]        [Component]
   7171.42      5242.27       BLZ_CollBars
   3956.95      1373.25       BLZ_CathodeFlexes
   1502.86      1097.98       BLZ_Deckplate_In
  36662.16      6004.28       BLZ_SW_AboveBars
   2930.94      2461.33       BLZ_SW_BarLevel
   1435.80       561.74       BLZ_SW_BelowBars
   1357.28        70.57       BLZ_SW_CradlesFlange
  10802.30       336.71       BLZ_SW_CradlesWeb
   7843.77      1086.40       BLZ_SW_DeckPlate_Out
   6674.86       432.24       BLZ_Shell_Floor
   1252.41       928.74       BLZ_EW_BelowBox
   1928.73       675.70       BLZ_EW_Box
    108.84       331.82       BLZ_EW_CradlesFlange
    420.19       333.48       BLZ_EW_CradlesWeb
   2092.54       911.78       BLZ_EW_Deckplate_Out
   9900.20      5292.81       BLZ_EW_InsideBox
   4665.44     31003.70       Heat leaving cathodic CV
      0.00                   Joule Heat outside cathodic CV
============================================================

ERROR CALCULATION
------------------------------------------------------------
  Ledge converged?             [-]    Yes
  Ledge Max Temperature error [oC]    8.88
  Ledge Max Iter. Disp.       [mm]    0.1
  Number of global iterations  [-]    35
  FEA Heat imbalance           [W]    2.83
  FEA Heat imbalance           [%]    2.81E-03
============================================================
```

Figure 6. Standardized output example.

3 Modernized Approach Features

We follow the recommendations of Arkhipov et al [6] and include the bath and the metal pad in the electrical problem to obtain a representative current distribution in the metal pad and an accurate anode voltage drop. However, the liquids are assumed to be isothermal at the operating temperature and are not part of the thermal domain. The liquids are split into a fixed part and a moving part that follows the ledge.

The latest generation ANSYS elements are used for the calculations. These elements are compatible with the high-performance computing solvers, including the Distributed Domain Solver (DDS) which we use to solve the full quarter model. The finite element mesh can be linear or quadratic, which enables a tetrahedral mesh to be used with an excellent accuracy for all the calculation domain, except for the ledge and the moving liquids that need to be structured due to the ledge repositioning logic.

3.1 Ledge Repositioning Logic

During preprocessing, auxiliary matrices and local coordinate systems are built and stored. This data structure is reused for every ledge moving iteration. This reduces considerably the overall time spent accessing the ANSYS database over the course of the global problem solution. The

data structure is built to be easily expanded, and several additional controls were implemented to overcome convergence difficulties with a particularly challenging lining design. These include for example:

- A ledge displacement relaxation factor by ledge zone (sidewall/end wall and lower/upper portions);
- An absolute displacement cut-off during a moving iteration, by ledge zone (sidewall/end wall and lower/upper portions).

The moving logic was generalized to an arbitrary number of elements through the thickness and for either linear or quadratic elements. The construction of the auxiliary matrices is based on the connectivity of the finite element mesh instead of the spatial position of the nodes, which makes the routines generic to any geometry with a structured ledge mesh. This feature can easily handle dissimilar side and end lining profiles – refer to Figure 7 – and arbitrarily shaped ledge profiles.

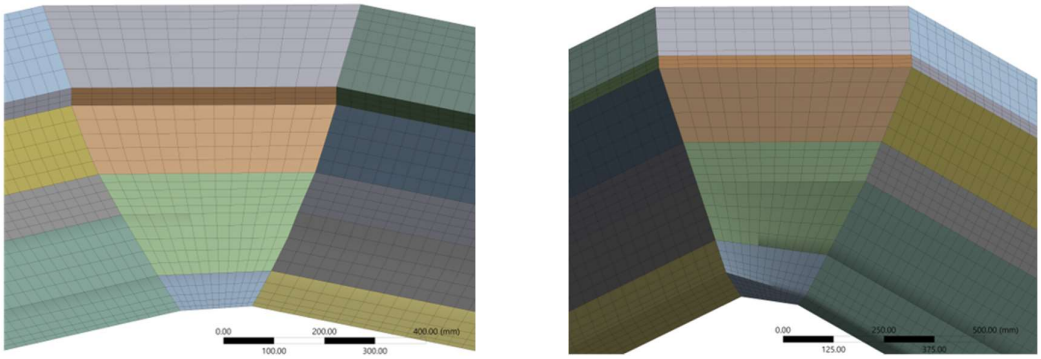

a) Structured, non-uniform corner ledge FE mesh, as seen from the inside of the cell.

b) Structured, non-uniform corner ledge FE mesh, as seen from the outside of the cell looking up.

Figure 7. Structured, non-uniform ledge FE mesh from dissimilar side and end profiles.

As the nodes within the ledge are repositioned to obtain the bath liquidus temperature at the interface with the liquids, the nodes in the moving liquids are also repositioned to maintain adequate element aspect ratios in order to obtain an adequate current distribution. An example for a quadratic mesh is shown in Figure 8.

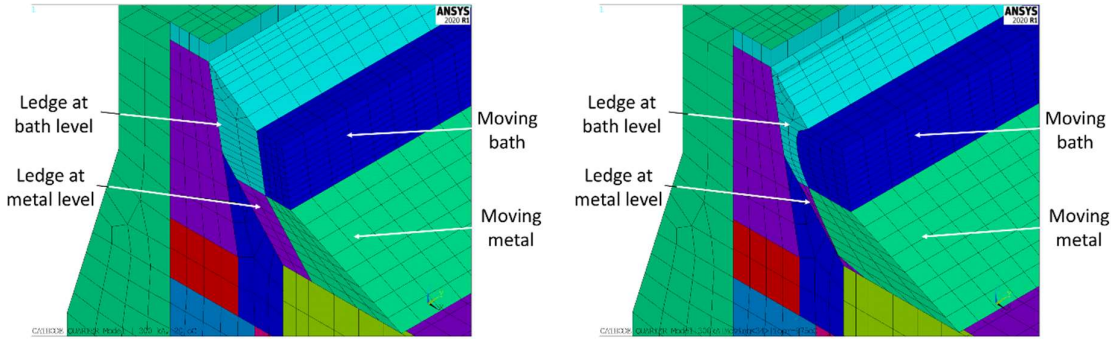

a) Initial mesh.

b) Converged ledge profile mesh.

Figure 8. Initial and final 2nd order FE mesh for ledge and moving liquids zones.

The convergence of the ledge profile is based on the infinite norm of the temperature difference with the liquidus and/or on the infinite norm of the iterative ledge displacement.

As previously mentioned, an important aspect of this work is that the ledge, the cathode and the metal pad have independent meshes that are reconnected by contact elements. This allows the ledge to freely move on the cathode surface irrespectively of the cathode topology. The ledge displacement outwards is constrained only by the external surface of the moving liquids zone, and inwards by the cell lining geometry.

3.2 Heat Balance Solution

The same approach than Dupuis [3] is used to converge the heat balance solution, which involves iteratively solving the thermal-electrical problem until the heat imbalance, *i.e.* the difference between the cell internal heat and the total heat losses, is less than the convergence criteria AND the ledge profile has converged. This scheme assumes a fixed bath chemistry. Therefore, for each global iteration, a new thermal-electrical solution is done, the voltage drops are obtained from the finite element solution, a new cell internal heat is calculated, the cell heat losses are integrated over the control volume, and the convergence metrics are calculated. If the global problem is not converged, a new operating temperature is calculated, and the ledge profile is repositioned, otherwise the solution is done and the postprocessing is performed.

The calculation of the cell internal heat is based on the APDL implementation of the steady-state cell voltage and heat balance routines used in the dynamic cell simulators ARC/Dynamic and Dyna/MARC [7].

A generic iterative heat balance convergence scheme was implemented to converge both the superheat and the ledge profile at the same time. The global convergence was shown to be slow but robust, as seen in Figure 9. A standard Newton-Raphson scheme is also available, but it was found to be prone to divergence for the challenging lining design mentioned previously. The user can however activate it for well-behaved problems.

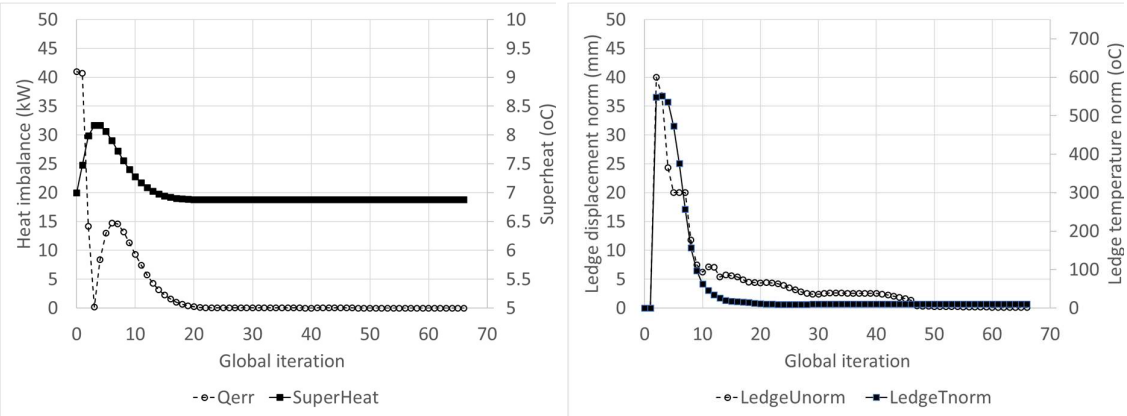

a) Superheat and heat imbalance. b) Ledge convergence infinite norms.

Figure 9. Global heat balance and ledge profile convergence for the linear mesh case.

3.3 Standardized Output

The detailed heat losses reported in the standard output file are independent of the heat losses calculated for the complete cell used for converging the heat balance. The definition of these

surfaces is entirely up to the User, which is particularly useful when planning a measurement campaign for model validation, The output surfaces can therefore be defined to match what can be measured in practice, and to the level of details appropriate for the task at hand.

Referring to Figure 6, the `[Component]` column corresponds to a named selection on which the heat flow is integrated, except for two lines:

- `Heat leaving cathodic CV`
  Heat flow leaving the defined cathodic control volume. This contribution is used in the cell heat balance.

- `Joule Heat outside cathodic CV`
  Joule heat in the elements outside the control volume. This heat input is not considered in the cell heat balance.

In this work, the control volume boundary is at the end of the cathodic flexes, and there are no elements outside the cathodic control volume. These two contributions are also calculated for the anode panel.

4 Model Results With the Standard Ledge Topology

The demonstration model used by Dupuis (refer, for example, to [2]) was rebuilt in the modernized environment with the standard ledge topology as seen in Figure 8. In this configuration, the ledge toe moves horizontally on the cathode surface. For a direct comparison, a linear mesh was first used.

The heat balance problem was solved with both platforms using the same material properties, the same boundary conditions and the same key simulation parameters:

Table 1. Comparison case main process parameters.

Parameter	Unit	Value
Cell amperage	[kA]	300.0
Excess [AlF_3]	%	10.825
Dissolved [Alumina]	%	2.5
[CaF_2]		3.0
[LiF]		0.0
[MgF_2]		0.0
External voltage	mV	200.0
ACD	cm	5.0

The main heat balance and computational results are summarized in Table 2.

Table 2. Comparison case main heat balance results.

Result	Original Dupuis	Hatch Modernized	Unit
Operating temperature	974.72	974.88	ºC
Liquidus temperature	967.99	967.99	ºC
Superheat	6.73	6.88	ºC
Cell internal heat	639.5	642.1	kW

Result	Original Dupuis	Hatch Modernized	Unit
Anode heat losses	236.3	234.4	kW
Cathode heat losses	403.5	407.6	kW
Total cell heat losses	639.8	642.1	kW
Heat imbalance	0.037%	0.000%	kW
Anode voltage drop	334.3	339.3	mV
Cathode voltage drop	287.2	290.4	mV
Ledge temperature norm	20.8	10.6	ºC
Ledge displacement norm	1.0	0.1	mm

The converged ledge profiles are compared in Figure 10, with cyan being for the original methodology and purple for the modernized version. The profiles are almost identical at the sidewall, but the ledge toe in the modernized version is longer in the corner.

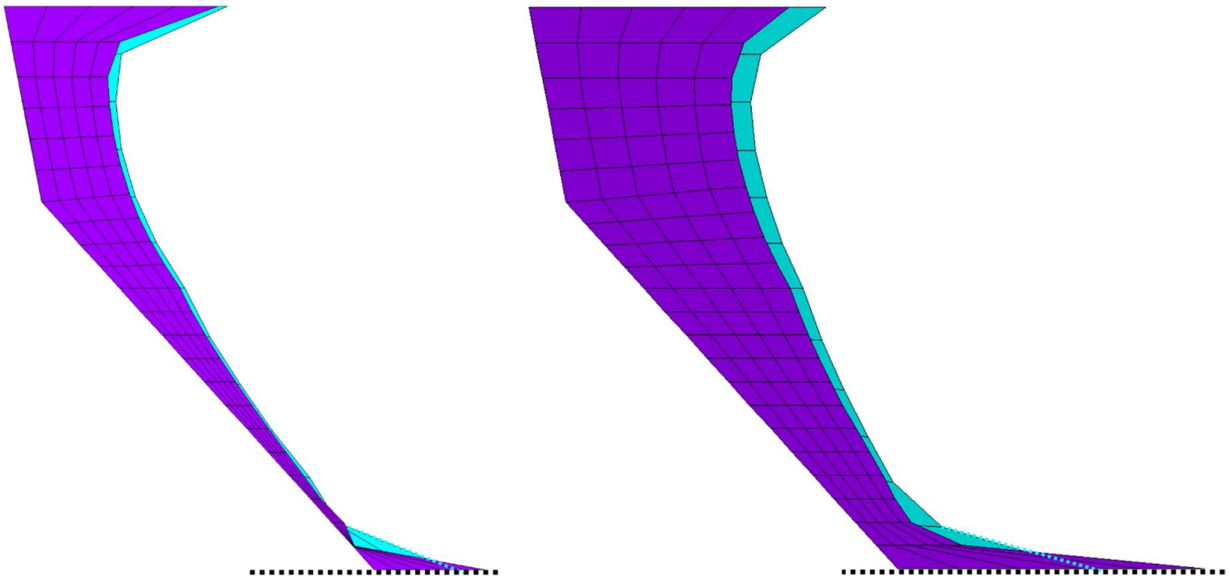

a) Sidewall. b) Corner section at 45º.

Where: Cyan = original (2 linear elements across ledge thickness) / Purple = modernized (5 linear elements across ledge thickness).

Figure 10. Ledge profiles for the comparison case.

It was found that the ledge toe is limited by the corner of the original version due to the construction of the corner mesh on the cathode block. This is shown in Figure 11 a) where the green ledge is constrained by the dotted white line. This constraint does not exist in the modernized version in Figure 11 b) due to the use of contact-target elements between distinct parts.

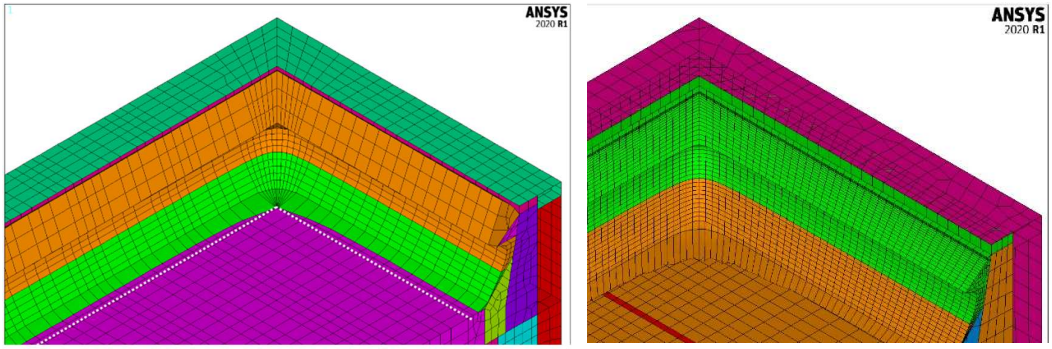

a) Original Dupuis – corner ledge movement is limited by the cathode panel-to-ledge mesh connectivity.

b) Modernized – ledge movement not hindered by the cathode panel mesh.

Figure 11. Corner ledge profile meshes for the comparison case.

For the modernized model, the ledge was compared at the same superheat for the linear mesh and a quadratic mesh with only 2 elements through the thickness. The quadratic mesh is shown in Figure 8. The obtained profiles are essentially identical, as shown on Figure 12 a) for the sidewall, and on Figure 12 b) for a cut through the corner. This built-in capability allows the User to easily perform mesh independence tests to determine the appropriate discretization scheme for the task at hand.

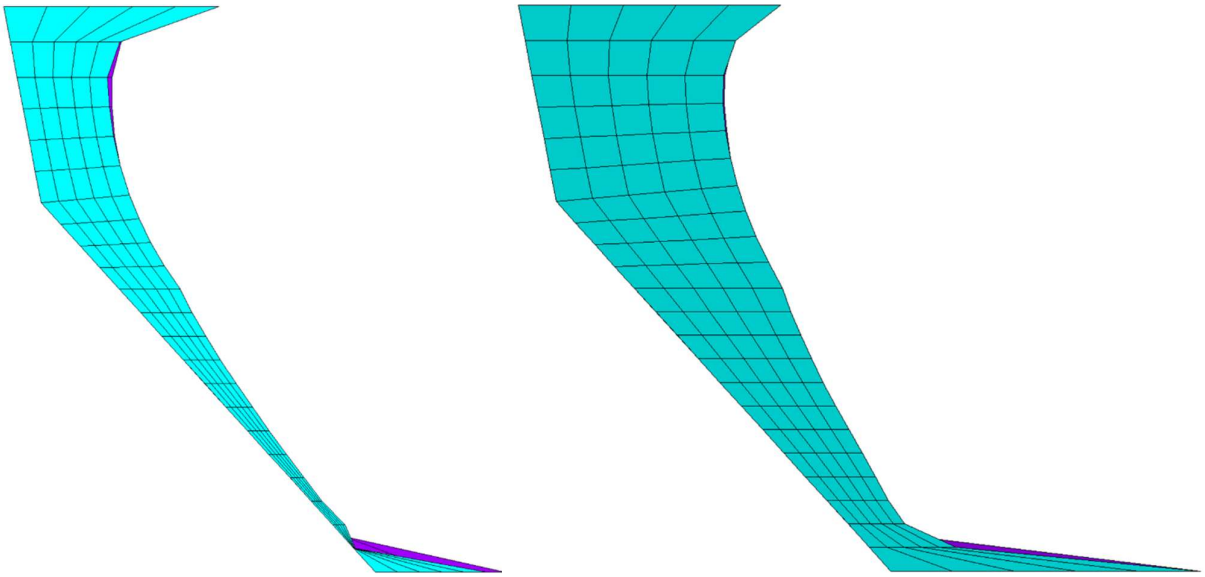

a) Sidewall.

b) Corner section at 45º.

Where: Cyan = linear mesh (5 elements across thickness) / Purple = quadratic mesh (2 elements across thickness).

Figure 12. Linear and quadratic ledge profiles for the comparison case.

For reference, the machine used to solve the modernized models is a 28 core Intel(R) Xeon(R) Gold 6240 CPU @ 2.60GHz with 128GB of RAM. The ANSYS WB database processing was done using 4 cores in Shared Memory Processing mode (SMP) while the solution was done using

the ANSYS sparse Distributed Domain Solver (DDS) with all 28 cores. The maximum memory used was 30 GB of RAM. The elapsed time is detailed in Table 3. It can be seen that the modernized approach using auxiliary matrices is very efficient since most of the elapsed time is spent computing finite element solutions. In fact, the total elapsed time spent to reposition each and every node defining the ledge was less than ten (10) seconds per global solution iteration.

Table 3. Modernized full quarter heat balance and ledge convergence computational data.

Task	**Elapsed time (min)**	**Elapsed time (%)**
Process ANSYS WB database	3.9	2%
Solve the global heat balance problem	172.5	98%
Elapsed time spent moving ledge	*3.5*	*2%*
Elapsed time spent preparing solution	*11.4*	*6%*
Elapsed time spent computing solution	*143.8*	*82%*
Elapsed time spent postprocessing solution	*1.6*	*1%*
Elapsed time spent post-processing model	*12.2*	*7%*
Total	176.4	100%
Parameter	**Value**	**Unit**
Number of degrees of freedom	534,079	DOF
Number of global iterations	66	iterations
Ledge temperature infinite norm	10.6	ºC
Ledge displacement infinite norm	0.1	mm

For the original methodology, which builds the model from scratch, the elapsed time breakdown in shown in Table 4. Two-thirds of the time is spent in the preprocessor for building the model, moving the ledge and updating the boundary conditions. The machine used to solve this model has 2 cores Intel i5-6300U CPU @ 2.40 GHz processors used in Shared Memory Parallel (SMP) processing.

Table 4. Original full quarter heat balance and ledge convergence computational data.

Task	**Elapsed time (min)**	**Elapsed time (%)**
Elapsed time spent pre-processing model	58.9	65%
Elapsed time spent solution - preprocessing	0.2	0%
Elapsed time spent computing solution	29.7	33%
Elapsed time spent solution - postprocessing	0.0	0%
Elapsed time spent post-processing model	1.8	2%
Total	90.7	100%
Parameter	**Value**	**Unit**
Number of degrees of freedom	162,506	DOF
Number of global iterations	17	iterations
Ledge temperature infinite norm	20.8	ºC
Ledge displacement infinite norm	1.0	mm

5 Novel topology

The Authors encountered a challenging lining design that would result in the standard ledge repositioning algorithm to diverge. For this design, the ledge tends to grow far in the corner and

then melt back at the sidewall and at the end wall. Near the corner, the side ledge and the end ledge therefore move in zones that have very low thermal gradients, such that one node would move towards the wall and the neighboring node would move towards the cell center, creating "ledge spikes". Once these spikes were formed, the global solution diverges.

The cause of the problem is thought to be a combination of cold cathodes, a cold corner and a very insulated end wall. After many trials and refinements to the controls of the allowable ledge displacement, further analysis revealed it would never be possible to converge the ledge with the standard algorithm since there would always be at least one ledge slice that has two possible solutions for the position of the ledge toe. This is schematically show in Figure 13**Error! Reference source not found.**.

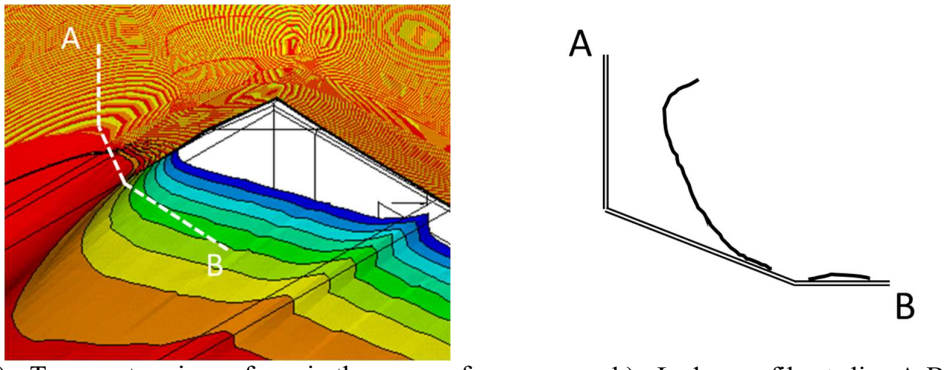

a) Temperature isosurfaces in the corner, from white (very cold) to blue (cold), to hot (red).

b) Ledge profile at slice A-B.

Figure 13. Challenging corner design for standard ledge repositioning algorithm.

A new ledge repositioning topology was devised that makes the ledge move normal to a set of arbitrary planes, as shown in Figure 14 b). The initial solution is done with the elements on the cathode surface as thermal-only frozen ledge (Figure 14 a). Once the ledge thickness on the cathode surface has been reduced to a prescribed minimum, the elements are switched to liquid metal and now conduct electricity between the metal pad and the cathode blocks surface. If the element surface temperature is under the bath melting temperature, the stack of underlying moving elements is turned back to thermal-only ledge properties. The applied thermal boundary conditions are updated at every moving iteration depending on the element status, while the physics of the contact-target element pairs used to connect the different parts is modified accordingly.

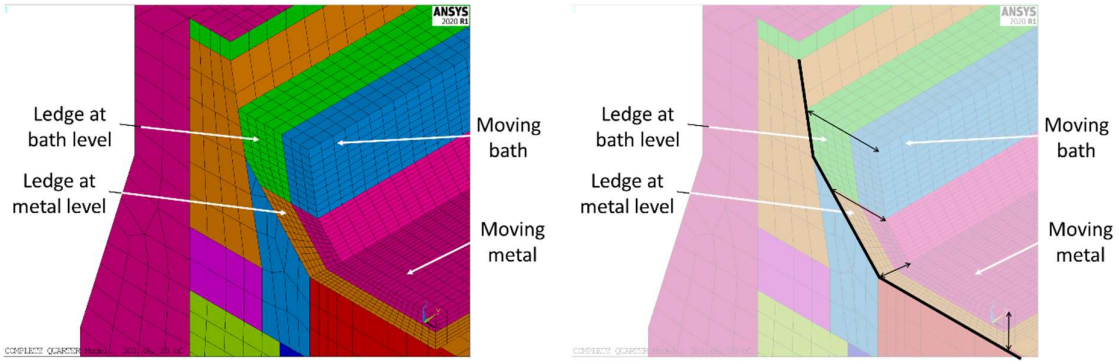

a) New topology initial mesh.

b) New topology ledge displacement direction.

Figure 14. New ledge repositioning initial mesh and ledge displacement direction.

The construction of the ledge repositioning auxiliary matrices is identical to the standard topology since the data acquisition is based on the finite element connectivity of the structured ledge and moving liquids. Additional information was added in the existing data structure to track the status and the specific information required to process the ledge elements on the cathode surface.

The demonstration lining design was modified with adjustments to material properties and boundary conditions to obtain similar issues to the real-life stubborn lining design. The changes made were designed to obtain a cold cathode and a hot end wall. To simplify the problem, the problem was solved only for the ledge profile at a constant superheat of 6.5 ºC.

The obtained ledge convergence curves are shown in Figure 15. The standard ledge topology does not converge and oscillates up to the prescribed maximum number of global iterations, while the novel topology converges within 33 iterations.

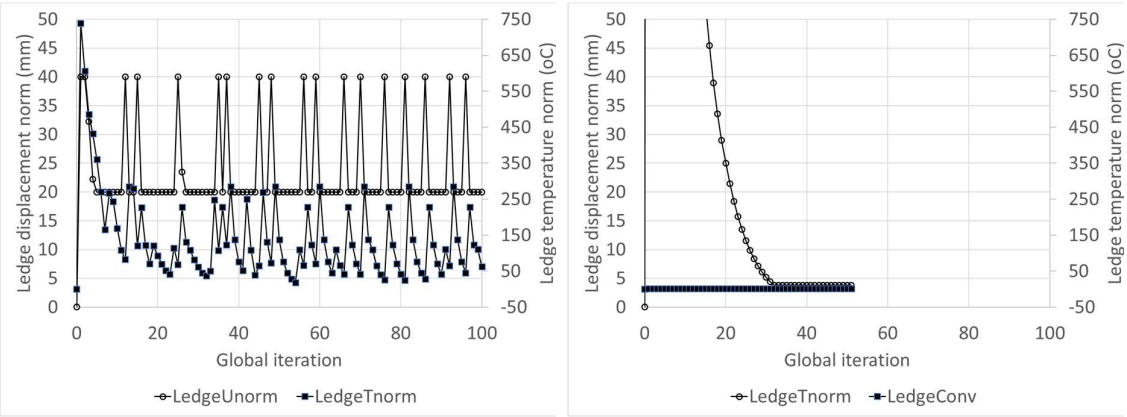

a) Standard topology. b) New topology.

Figure 15. Problematic lining ledge convergence curves.

The resulting ledge profiles are compared in Figure 16. Despite the whole ledge that should have disappeared at the end wall, a “ledge spike” appears for the standard topology in a region of low thermal gradient. The current flow into the center of the block is low due to the split bar design with castable in the middle of the slot and the thermal flux pulled by the collector bars is the lowest.

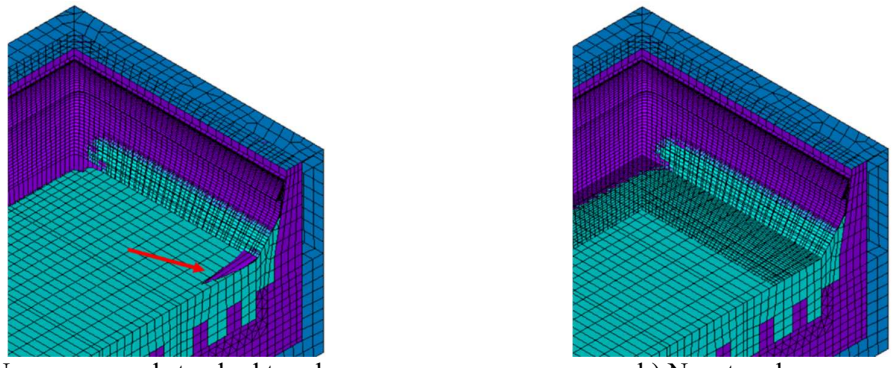

a) Non converged standard topology. b) New topology.

Figure 16. Problematic lining ledge profiles.

6 Discussion

The novel topology allows solving problems that cannot be converged by the standard approach, particularly when the lining design results in zones of low thermal gradient on the cathode blocks. The ledge toe profile calculated by both methods differs. It is clear from Figure 17 that the standard topology (in purple) produces elongated elements at the ledge toe while the novel topology (in cyan) results in a smooth and thin layer of ledge at the toe.

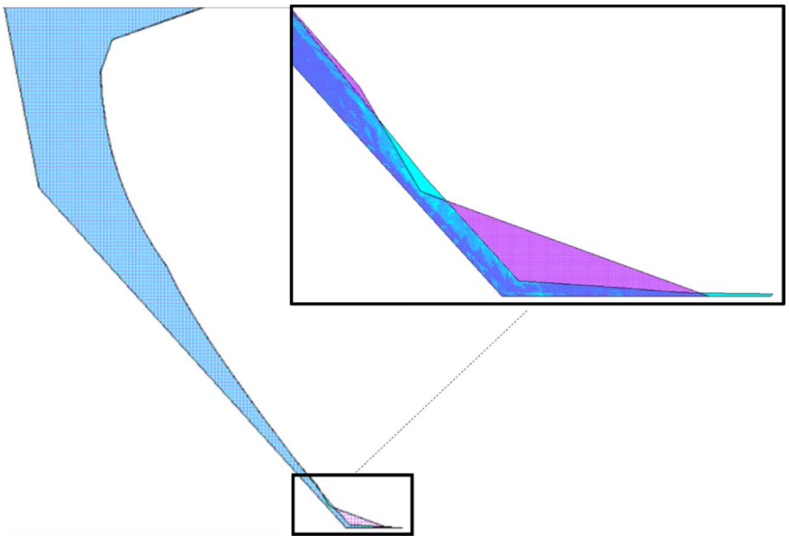

Where: Cyan = novel topology / Purple = standard topology.

Figure 17. Comparison of ledge profile elevation with standard and novel topology.

While the ledge profile solution appears better in elevation, one of the drawbacks of the novel topology the "checkerboard" pattern of the ledge toe due to the fixed horizontal discretization of the ledge. This is shown in Figure 18 for the standard lining design. This checkerboard pattern effect can be reduced (but not entirely avoided) by refining the FE mesh at the ledge over the cathode panel, and by using a different meshing scheme in the corner.

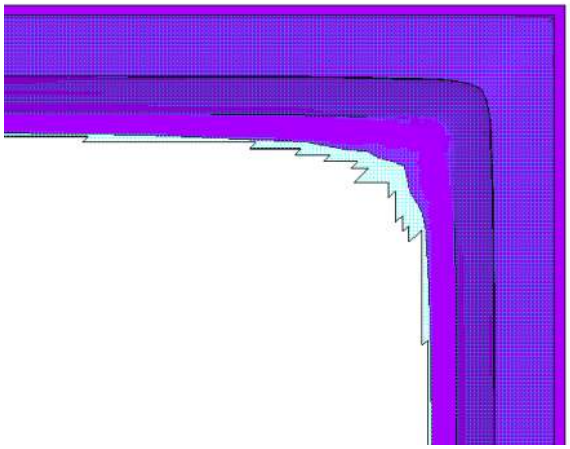

Where: Cyan = novel topology / Purple = standard topology.

Figure 18. Comparison of ledge profile plan view with standard and novel topology.

7 Conclusion

A modernized approach to thermal-electrical finite element modeling of the cell heat balance was developed in the commercial software ANSYS 2020 R1. The new workflow is based on a combination of an interactive ANSYS/Workbench session, user-edited input text files, and generic APDL scripts running in the background. The main limitations of the original approach were eliminated, and the use of the most recent ANSYS element technology enables leveraging the high-performance parallel computing solvers, including the Distributed-domain sparse solver (DDS).

The modernized model was compared to the original approach for a complete quarter cell heat balance and ledge profile solution, and the results were found to be very similar. Convergence of the ledge profile was done for a linear and a quadratic mesh with identical results.

A novel ledge topology was developed that is based on the displacement of the ledge nodes orthogonally to any arbitrary set of planes. The new topology allows the convergence of otherwise impossible to converge problems.

Further work includes experimental validation of the heat balance model and assessment of the ability of the novel ledge topology to predict accurately the position of the ledge toe.

8 References

1. Marc Dupuis & I. Tabsh, Thermo-electric coupled field analysis of aluminium reduction cells using the ANSYS parametric design language, *Proceedings of the ANSYS fifth international conference*, Vol 3, 1991, p.1780-1792.
2. Marc Dupuis, Thermo-electric design of a 400kA cell using mathematical models: a Tutorial, *Light Metals* 2000, p. 297-302.
3. Marc Dupuis, Computation of Aluminium Reduction Cell Energy Balance using ANSYS® Finite Element Models, *Light Metals* 1998, p.409-417.
4. Marc Dupuis, Computation of accurate horizontal current density in metal pad using a full quarter cell thermo-electric model, *Proceedings of CIM* 2001, p.3-11.
5. Marc Dupuis, How to limit the Heat Loss of Anode Stubs and Cathode Collector Bars in Order to Reduce Cell Energy Consumption, *Light Metals* 2019, p.521-531.
6. Alexander Arkhipov et al., Review of Thermal and Electrical Modelling and Validation Approaches for Anode Design in Aluminium Reduction Cells, *Proceedings of the 36th Conference and Exhibition* ICSOBA, Belém, Brazil, *TRAVAUX* 47, p.589-605.
7. I. Tabsh, Marc Dupuis and A. Gomes, Process Simulation of Aluminum Reduction Cells, *Light Metals* 1996, 451-457.